Journal of the Serbian Chemical Society
JSCS@tmf.bg.ac.rs • www.shd.org.rs/JSCS
*J. Serb. Chem. Soc.* *90* (4) 431–446 (2025)
*JSCS–5398*
*Original scientific paper*
Published 24 April, 2025

# Molecular dynamics simulation of uranium nitride oxidation

ALEXANDER Y. GALASHEV[1,2]*, YURII P. ZAIKOV[1,2], KSENIYA A. ABRAMOVA[1,2], OKSANA R. RAKHMANOVA[1,2] and YURII S. MOCHALOV[3]

[1]*Institute of High-Temperature Electrochemistry, Ural Branch of the Russian Academy of Sciences, Yekaterinburg, Russia,* [2]*Ural Federal University named after the first president of Russia B.N. Yeltsin, Yekaterinburg, Russia and* [3]*Joint-Stock Company "Proryv", Moscow, Russia*

(Received 26 September, revised 5 October, accepted 24 November 2024)

*Abstract*: A molecular dynamic simulation of the uranium mononitride (UN) oxidation in an Ar–O medium in the temperature range of 373–2073 K is performed. The study is performed for UN particles with a crystalline and amorphous structure at an oxygen concentration in the gas mixture of 22.5 mol. %. The most efficient oxidation for an amorphous particle occurs at lower temperatures than that for a crystalline particle. Unlike crystalline fragments, amorphous particles undergo more severe fragmentation when they bind to oxygen. Fragmentation of UN particles is one of the main factors regulating the oxidation of finely dispersed media. The oxidation of a UN particle begins from its surface and in the case of an amorphous particle occurs faster than when the particle is crystalline. The process of particle fragmentation is facilitated by the penetration of oxygen atoms inside the particle. An increase in the oxygen concentration in the gas mixture stimulates the oxidation process. The structural changes in the system are investigated by constructing the partial radial distribution functions. The many-body U–N interactions prevent nitrogen escaping into the gaseous environment.

*Keywords*: amorphous and crystalline fragments; argon; calculation; oxygen; structure.

## INTRODUCTION

The pyrochemical technology for reprocessing spent nuclear fuel (SNF) includes several stages, among which a high-temperature processing (HTP) of SNF is at the beginning of the entire technological chain and is the main stage. The HTP stage includes several steps. At the first step, the SNF pellets are dispersed and separated from the fuel rod cladding using the high-temperature nitriding procedure.[1] At the second stage of HTP, the components of nitride SNF

* Corresponding author. E-mail: alexander-galashev@yandex.ru
https://doi.org/10.2298/JSC240926110G

are oxidized in an atmosphere of dry oxygen and argon with the formation of oxides of fissile materials and part of the fission products. The conversion of UN to $UO_2$ is one of the preparatory operations before conducting spent nuclear fuel recovery procedures. The need to convert spent nitride nuclear fuel into oxides arises from the fact that the direct reduction of UN during the electrolytic process in molten salt is incomplete, and $UO_2$ is more suitable for pyrochemical reprocessing.

High thermal conductivity and melting point values at high densities make uranium mononitride (UN) one of the best fuel components for the fourth-generation nuclear reactors.[2] The advantages of nitride fuel over oxide fuel allow the fuel to operate at higher burnups. The increased formation of interstitial N atoms and U vacancies leading to a hyperstoichiometry of nitride fuel at elevated temperatures does not have a significant effect on its thermal and mechanical properties.[3] At the same time, fission gas atoms have low solubility in the fuel matrices. The release of these gases leads to swelling of the fuel and deterioration of its thermal conductivity. The energy barrier to the diffusion of released gases decreases when moving from pure UN to the disordered $U_{0.5}Pu_{0.5}N$.[4] Moreover, the energy barrier for Kr diffusion (0.30–1.25 eV) turns out to be lower than that for Xe diffusion (0.50–1.75 eV) due to the smaller size of the Kr atom.

The oxidation of real powdered UN with a surface area of 0.2–0.4 $m^2\ g^{-1}$ in the temperature range of 503–543 K resulted in the formation of an amorphous product with the composition of $UO_3N_{0.2–0.4}$, which releases nitrogen slowly and recrystallizes into $\alpha$-$UO_3$.[5] At the same time, X-ray studies showed that $U_2N_3$ and $UO_2$ are formed as intermediate oxidation products. It is known that $UO_2$ can be reduced to metallic uranium with a yield of up to 99.7 %.[6] However, this result cannot be obtained using the electrolytic method if the reduction of the spent nitride fuel is carried out.

Based on density functional theory (DFT) calculations, it was shown that in the pressure range of 0–1000 kbar, uranium is capable of reacting with nitrogen to form various U–N compounds in the form of semiconductors and metals.[7] A new tetragonal phase for $UN_2$, more stable than the known phases for this compound, was found. In addition, the new stoichiometry of $U_3N_5$ was shown to be stable at atmospheric pressure. At pressures above 500 kbar, not only the phases with a high nitrogen content ($UN_4$, $UN_3$), but also the phase with a high uranium content ($U_2N$), which initially has an orthorhombic structure, turned out to be stable. The pressure-induced phase transition of $U_2N$ to the monoclinic phase occurs at a pressure of 980 kbar. Both the orthorhombic and monoclinic $U_2N$ structures consist of one-dimensional zigzag U-chains, which play an important role in stabilizing U-rich compounds. All phase transitions (with the exception of the transition to $UN_2$) are first-order transitions and occur with a change in volume.

The chemical bond in the uranium dinitride ($UN_2$) molecule is not studied properly. This is mostly due to the complexity of the electronic structure of the uranium atom, the quantum mechanical calculation which requires taking into account both electronic correlation and relativistic effects. Particularly large discrepancies are observed in the calculations of excitation energies when different theoretical approaches are used.[8–10]

The valence shells of early-middle actinides (5f6d7sp from Pa to Pu) are energetically close to each other, and the orbital radii regularly increase with the principal quantum number.[11] The formation of multiple 5f, 6d, 7sp bonds with partner atomic orbitals (AO) is characteristic of these actinides. The different occupancy of the 5f AO in these elements is due to the strong electron repulsion between the 5f, 6d and 6p shells, which are located in close radial regions.

Studying the electronic structure and bonds in individual ions allows us to better understand the formation of bonds between the same elements in a bulk material. The uranyl ion ($UO_2^{2+}$) predominantly forms complexes with oxygen-containing ligands that have donor properties with respect to the central cation $UO_2^{2+}$. The stability and electronic structure determine the stability of the bonds in the complex. The U–O bond length in $UO_2^{2+}$ is smaller (1.704 Å) than the U–N bond length in $UN_2$ (1.736 Å).[12] The linear form of each of these structures is the most stable. The transition to the bent form of the uranyl or $UN_2$ molecule causes the destabilization of the U $6p_{3/2}$ orbitals, which is more pronounced for $UO_2^{2+}$. Although the study was performed for "naked" molecules, the results obtained can also be applied to complexes with very weak ligand fields.

The geometric structure of $NUO^+$ appears to be linear with possible additional $N_2$ ligands in the second coordination sphere of the type $[NUO•(N_2)_5]^+$.[13] The dynamics of this complex is characterized by high N–U stretching modes and relatively low U–O modes. Stabilization of the complex occurs due to N≡U and U≡O triple bonds. In $NUO^+$, the interaction between more covalent N–U bonds with more ionic U–O bonds is observed, with the terminal atoms effectively competing for U-5f, 6d and 7sp atomic orbitals. Here, the charge transfers from U to N and O occur in amounts of 0.4 and 1.2e, respectively.[13]

The aim of the present work is to study the stability of crystalline and amorphous UN particles immersed in a gas mixture of argon and oxygen, as well as to determine the optimal conditions for the oxidation of these particles, and to identify the influence of particle structure on their oxidation.

## MOLECULAR DYNAMICS MODEL

The oxidation of UN was studied using two types of models. In one of them, crystalline UN particles, and in the other, amorphous UN particles were placed in a gaseous mixture of argon and oxygen. Consideration of particles with regular (crystalline) and irregular (amorphous) structures surrounded by a gaseous Ar–O medium was executed to study the influence of the particles structure on the process of their oxidation. The details of preparation pro-

cedure of the simulated systems "UN crystalline/amorphous particle in the Ar–O gaseous medium" are presented in the Supplementary material to this paper.

Taking into account that there are no experimental data on the reflection of gas atoms from the wall, in our model, the Maxwellian reflection boundary condition was used as the boundary condition, acting on all walls of the rectangular cell with the accommodation coefficient equal to 0.5. Modelling at the predominantly high temperatures of the gas medium with such conditions led to the formation of random gas flows that acted on the solid UN particle. As a result, the UN particle acquired both translational and rotational motions. Such behaviour of the particle in the argon–oxygen mixture was largely represented by the behaviour of a real particle in a gas flow and increased its adsorption capacity.

The principal part of the calculations was executed in the NVT ensemble at different temperatures from the range of $373 \leq T \leq 2073$ K (for every temperature, a separate calculation was executed). The thermostat relaxation time was $\tau_T = 4$ fs. The model contained 3172 atoms: 1772 Ar, 400 O, 500 U and 500 N. The density of the system was 0.48 g cm$^{-3}$. The pressure in the gas medium did not exceed 500 bar. The total calculation time for the systems with amorphous/crystalline UN particle for every temperature was up to 1 ns with the time step for integrating the motion equations of $\Delta t = 0.1$ fs. The Verlet scheme was used in the calculations for integrating the equations of motion.[14]

The U–U, U–N and U–O interactions were described by many-body EAM potential, the concept of which is based on the "embedded atom" strong-binding model.[15,16] The interaction of crystalline or amorphous particle with components of gaseous medium as well as the interactions between gaseous components (Ar–O, Ar–U, Ar–N, Ar–Ar, O–O, N–O) were described using the Lennard–Jones potential with parameters taken from.[17] These data are summarized in Table I.

TABLE I. Parameters of the Lannard–Jones potential[17]

| Bond | $\varepsilon$ / eV | $\sigma$ / Å |
|---|---|---|
| Ar–O | 0.0103 | 3.385 |
| Ar–U | 0.00314 | 3.192 |
| Ar–N | 0.00929 | 3.537 |
| N–O | 0.00929 | 3.512 |
| Ar–Ar | 0.0104 | 3.41 |
| O–O | 0.0103 | 3.36 |

During the simulation, it was revealed that due to the use of the EAM potential, N atoms are strongly bound to U atoms. As a result, nitrogen atoms do not break away from uranium atoms even at the highest temperatures at which the calculations were performed. At the same time, the O atoms, also interacting with the U atoms according to the appropriately selected EAM potential, actively bonded with the uranium atoms. To demonstrate the stabilizing effect of many-particle interactions at the final stage of simulation (when the duration of the calculation was 220 ps), the EAM interaction between the U and N atoms was replaced by a potential built on the basis of the Morse potential function.[18] The description of the potential details as well as potential parameters are presented in the Supplementary material.

DFT calculations showed that in the process of removing oxygen from $UO_2$, the reduction process is enhanced by the appearance of electrical conductivity in the recovered material. More precisely, electrical conductivity appears when the composition $U_2O_3$ is reached, which initiates direct reduction of this oxide.[19] To establish how strongly the concentration of oxy-

gen in the gaseous medium affects the degree of oxidation of UN particles, another series of calculations were carried at $T$ = 973 K, with adding 100 (oxygen concentration 26.7 mol. %), 200 (30.4 mol. %), 300 (33.8 mol. %) and 400 oxygen particles (maximum oxygen concentration of 36.8 mol. %). When the oxygen concentration in a Ar–O gas mixture was 36.8 %, the formation of the $U_2O_3$ compound became possible.

Additional oxygen was added into the system sequentially through the upper edge of the MD cell, one particle every 0.2 ps. When the required number of oxygen atoms was added, a relaxation MD calculation was performed for 100 ps to equilibrate the system. Then, the main calculation was carried out with the new number of O atoms in the system.

The content of bonds in the system was monitored using a special algorithm we developed, which allowed us to determine which U atoms formed a U–O bond. The algorithm was realized as follows. First of all, it analysed coordinates of all atoms of the system at equal time intervals (5 ps). Second, it was assumed that a bond between the U and O atoms was formed if the distance between these atoms became less than 3.3 Å. This parameter of connectivity between these atoms was determined while studying the stability of $UO_{2-x}$ hypostoichiometric compounds.[20] Third, the operation of the algorithm was based on storing a list of distances where $r \leq 3.3$ Å, along with the numbers of atoms between which the selected distances were formed. The formed bonds were determined by processing the entire list based on the stored numbers of the selected atoms. The minimum and maximum (just 3.3 Å) distances in the formed bonds were also determined. Finally, the number of O atoms forming bonds with U atoms was visually represented in relative units or percentages relative to the total number of O atoms in the system.

All calculations were performed with the use of the open-source program code for MD simulation LAMMPS (large-scale atomic/molecular massively parallel simulator)[21] on a URAN cluster-type hybrid computer at the N. N. Krasovskii Institute of Mathematics and Mechanics UB RAS with a peak performance of 216 Tflop/s and 1864 CPU.

## RESULTS AND DISCUSSION

Fig. 1a shows the configuration of the system with an amorphous UN fragment in the Ar–O gas mixture obtained at a temperature of 923 K, at time of 470 ps. In the model, fragmentation of the UN nanoparticle occurs. Many small fragments separated from the particle, although its larger part was also preserved. The UN particle has lost its initial spherical appearance, and the surface of its remaining part has acquired a “pockmarked” shape. While Ar atoms are uniformly distributed throughout the volume of the MD cell, the O atoms preferentially tend to occupy positions near UN fragments and, especially, near the larger particle fragment. However, at this initial stage of oxidation, the detachment of N atoms from the UN fragments is not observed.

Fig. 1b and 1c provide information about the state of a microheterogeneous system containing an amorphous (Fig. 1b) and a crystalline (Fig. 1c) UN fragment at a temperature of 1023 K and a time of $t$ = 260 ps. Argon atoms are not shown in the figure to clarify the fragmentation details. Both the amorphous and crystalline UN particles are subjected to fragmentation, with a tendency to retain a larger UN fragment. The larger remaining particle and the resulting clusters are surrounded by oxygen. There is noticeably more unbound oxygen, and, conver-

sely, there are fewer small UN clusters in the presence of crystalline formations in the system. Consequently, the processes of fragmentation and oxidation in a system with an amorphous particle occur more actively than in the presence of a crystalline particle of the same size.

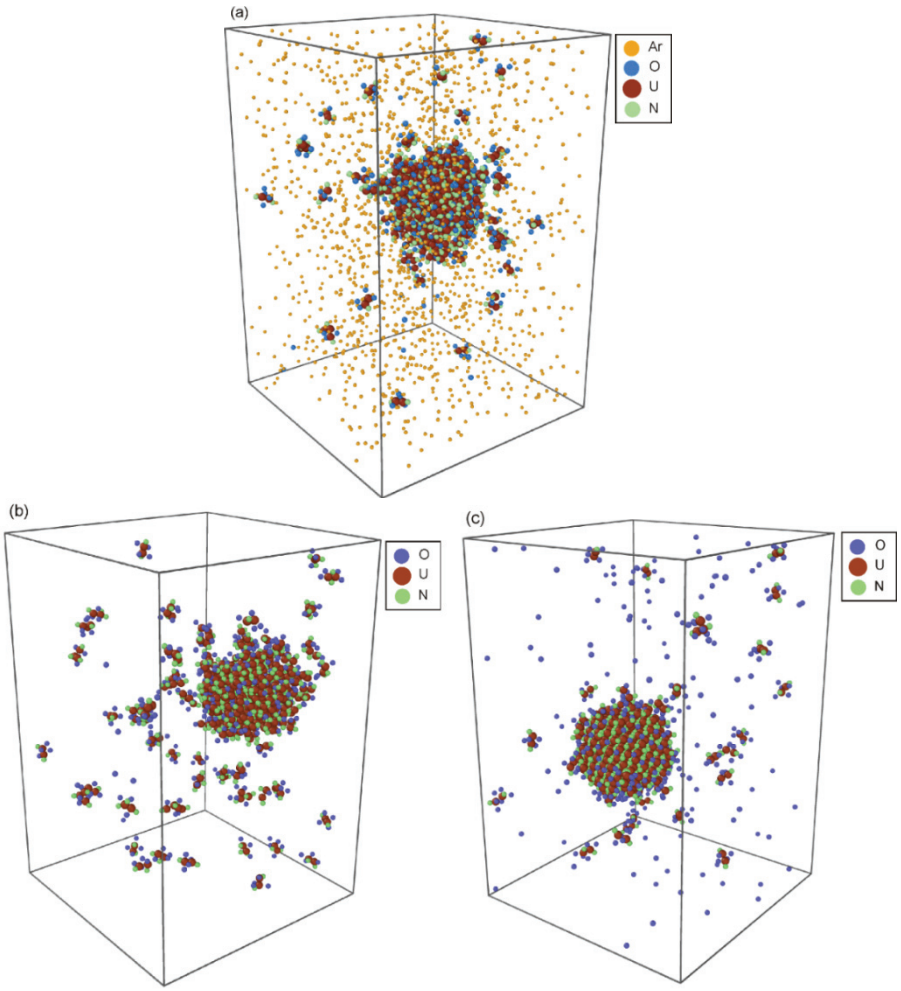


Fig. 1. Configurations of the system "UN fragments in a gaseous mixture of Ar+O": a) the amorphous particle configuration at a temperature of 923 K corresponding to the time moment of $t$ = 470 ps; configurations of: b) amorphous and c) crystalline UN particles at $T$ = 1023 K and $t$ = 260 ps; Ar atoms are not shown here for the visibility.

The difference in the structures of amorphous and crystalline particles can be seen in the form of partial radial distribution functions $g_{U–N}(r)$ characterizing the placement of N atoms around U atoms for these particles. The $g_{U–N}(r)$ functions

for crystalline particles have many pronounced peaks, and the number of these peaks decreases as the temperature of the system rises (Fig. 2). In contrast, the $g_{U–N}(r)$ functions for amorphous particles are characterized by only three obvious peaks.

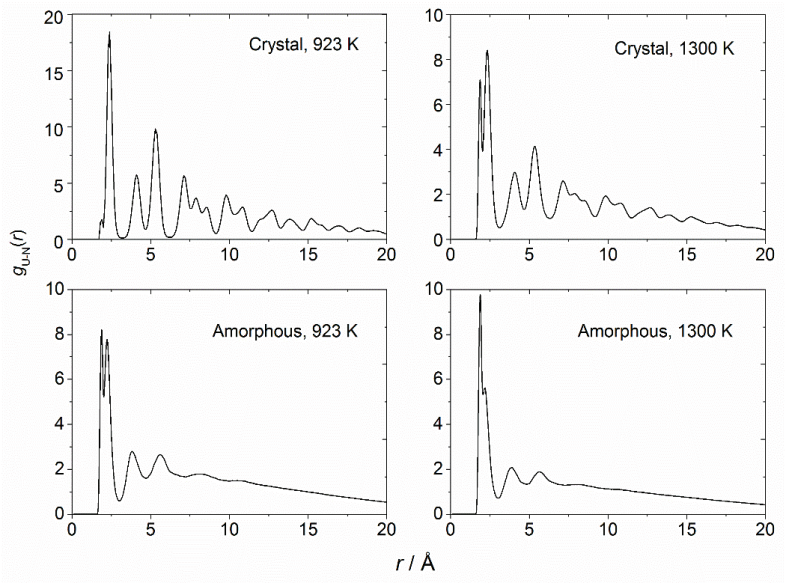


Fig. 2. Partial radial distribution functions $g_{U–N}(r)$ obtained by oxidation of crystalline and amorphous UN fragments in a gas mixture of Ar with 22.5 mol. % oxygen at different temperatures.

The intensity of the last two peaks decreases with the increase of temperature. The first, most intensive peak of the $g_{U–N}(r)$ function can be split or have a shoulder in both the amorphous and crystalline particles. For the crystalline particles, the intensity of the first peak of the $g_{U–N}(r)$ function decreases also with the increase of temperature, because the probability of finding N atoms around U atoms at nearest neighbour distances decreases. In the case of amorphous particles, the opposite trend may be observed, with the main peak of the $g_{U–N}(r)$ function splitting.

The time sequence of the formation of U–O bonds in systems with UN nanoparticles every 5 ps during the final part of the MD calculation at temperatures of 823 and 1273 K, is presented in Fig. 3. The initial interval (not shown in the figure) of the appearance of U–O bonds has a duration of 0.5 million time steps (50 ps). This initial interval is characterized by the rapid fragmentation of amorphous particles.

The left side of the figure presents the results of the formation of U–O bonds over time for the initially crystalline UN particles, and the right side gives the

information for the amorphous UN particles. The horizontal dashed line and the number above indicate the time-averaged number of U–O bonds ($n_b$) appearing in each case. It can be seen that the $n_b$ value for the crystalline nanoparticle at both temperatures is lower than that for the amorphous particle. Moreover, with the increase of temperature, the $n_b$ value rises noticeably for the crystalline fragment, whereas in the case of oxygen adsorption onto a fragment with an amorphous structure, the opposite effect can be observed.

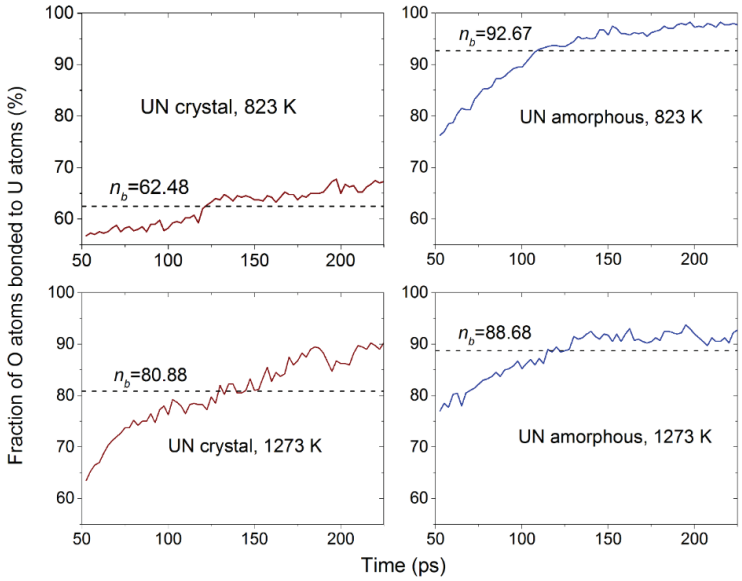


Fig. 3. Fraction of O atoms bonded to U atoms for initially crystalline and amorphous UN particles at different temperatures; the horizontal dashed line and the number above indicate the $n_b$ time-averaged number of U–O bonds appearing in each case.

Fig. 4 shows the average number of attachments of O atoms to U atoms (or $n_b$) obtained after every MD run and presented as a percentage of the total number of oxygen atoms in the system. As can be seen from the figure, there is a significant difference in the oxygen adsorption on crystalline and amorphous particles. A relatively small amount of oxygen atoms, varying from 62 to 65 % of the total amount of oxygen (400 atoms) present in the system, is adsorbed onto the surface of the crystalline particle up to a temperature of 923 K. Next, there is a trend of a slight increase in the amount of adsorbed oxygen when the temperature reaches 1123 K, where the proportion of deposited oxygen is 69 %.

A subsequent rise in temperature causes an increase in the fraction of deposited oxygen atoms up to 82.7 % at a temperature of 1300 K. Then, up to a temperature of 1673 K, a high level of adsorbed oxygen is maintained, with its fraction fluctuating by around 6 %. A further increase in temperature to 2073 K

causes an almost linear reduction in the fraction of oxygen attached by the UN particle, so that the percentage of oxygen at this temperature becomes even lower than at 1123 K.

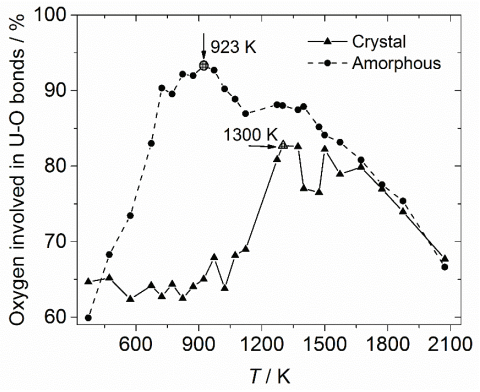


Fig. 4. The fraction of O atoms forming bonds with the U atoms of the crystalline and amorphous UN particles in relation to the number of all oxygen atoms in the system.

The fraction of oxygen attached to the amorphous UN particle immediately rises quickly when the temperature reaches 723 K (from an initial temperature of 373 K). Further, the growth rate of oxygen added to the amorphous particle slows down until it reaches a maximum at 923 K. After that, there is a decline in the amount of oxygen attached by the amorphous particle, leading to its local minimum at a temperature of 1123 K. The following increase in the fraction of adsorbed oxygen occurs up to 1400 K, and then a trend toward a rapid decrease (approximated by a linear decline) in attached oxygen appears. Moreover, an increase in temperature, starting from 1673 K, leads to similar values of the fraction of oxygen attached to the amorphous and crystalline particles. Uranium mononitride does not maintain its composition upon heating to its melting point $T_m$. The decomposition of UN begins much earlier, prior to reaching $T_m$. Uranium mononitride begins to decompose already at 1673 K. At this temperature, the nitrogen pressure caused by the decomposition of UN is only $10^{-3}$ Pa.[22] However, it is not the departure of N atoms from the nanoparticle that is important; rather, it is the loosening of its surface that leads to the softening of the surface vibrational modes. For particles smaller than 5 nm, the softening occurs at lower temperatures (by several hundred degrees) compared to macroscopic objects. The softening of vibrations leads to an increase in adsorption capacity per unit surface area.[23] Additionally, the surface of the particles becomes rough, further enhancing their adsorption capacity. These two factors begin to dominate at temperatures above 1673 K, while, conversely, the difference in the structure of the particles is levelled out. The identical behaviour in the adsorption characteristic of nanoparticles with different structures can be explained by changes in the factors influencing the adsorption of oxygen.

Thus, in a system with approx. the same quantity of crystalline and amorphous particles, the most productive temperature range for oxidation is 923–973 K.

The results of the study of additionally added oxygen effect into the system are presented in Fig. 5. The change in the fraction of bound oxygen for particles of both types showed that, in the case of a crystalline particle, each subsequent $n_b(T)$ dependence (obtained with a large number of oxygen atoms) is lower than the previous similar dependence. This indicates that the rate of U–O bonds formation in the system lags behind the number of sites prepared for oxygen adsorption. This may be due to the lack of available sites for oxygen inside the crystalline particle, as well as the lack of such sites on the surface of the particle and the resulting fragments.

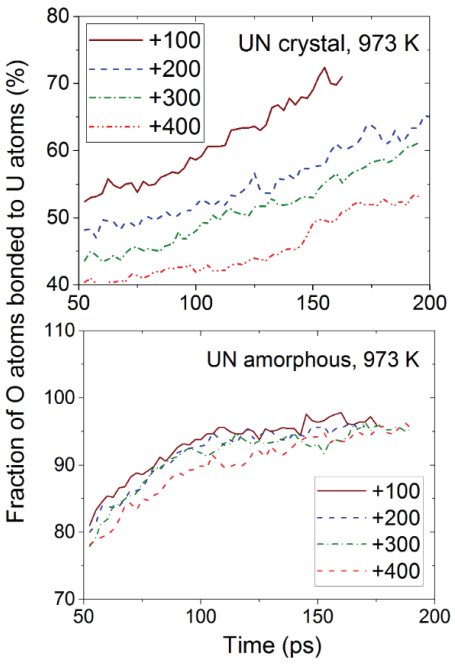


Fig. 5. Fraction of O atoms bonded to U atoms for initially crystalline and amorphous UN particle after sequential addition of oxygen to the system at different temperatures; numbers with a "+" sign indicate the number of added oxygen atoms.

A different result is observed for the amorphous particle. Here, enough potential sites for oxygen capture can be located both outside all the existing fragments and inside the not yet destroyed part of the particle. Therefore, each subsequent dependence of $n_b(T)$ for the amorphous particle follows a path quite close to the previous dependence (relating to a system with 100 fewer oxygen atoms).

The structure of a nanoparticle affects the packing of the attached oxygen. Fig. 6 shows the U–O partial radial distribution functions for two temperatures corresponding to the maxima of the $n_b$ distributions for crystalline and amorphous particles. At 923 K, the $g_{U–O}(r)$ function for a crystalline particle has a

large number of peaks, indicating a predominantly regular arrangement of oxygen atoms both around and within the particle. A similar function for an amorphous particle is characterized by only two intensive peaks, with the third peak being diffuse and weakly expressed. The connection between the structures of UN fragments and their oxygen environment and filling is also evident here.

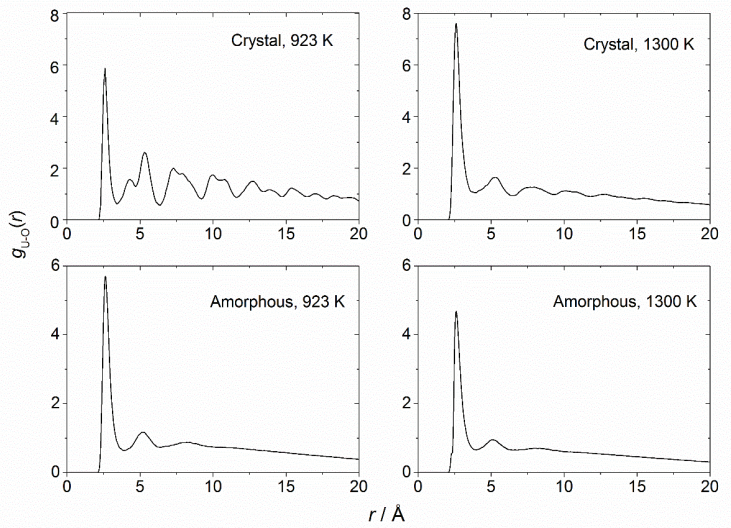


Fig. 6. Partial radial distribution functions $g_{U–O}(r)$ obtained by oxidation of crystalline and amorphous UN fragments in a gas mixture of Ar with 22.5 mol. % oxygen at different temperatures.

After heating the system to a temperature of 1300 K, the structure of the crystalline particle undergoes significant distortions, as a result of which the number of peaks in the $g_{U–O}(r)$ function is reduced, and the remaining peaks become blurred. In the corresponding function for the amorphous particle at 1300 K, only two peaks are detected, and the third peak, still present at a temperature of 923 K, becomes faintly noticeable. Thus, with the increase of temperature, there is a more noticeable disorder of the oxygen subsystem in the system with the crystalline UN particle. However, the oxygen subsystem in the system with the amorphous UN particle is also subject to structural disorder.

To visually summarize the results of the study, Fig. 7a shows the configuration of the system "amorphous fragments in a gas mixture Ar–O" close to the initial state (corresponding to a time of 20 ps) and the final configuration obtained in calculations with the U–N pair interaction potential and corresponding to a time moment of 685 ps.

The final demonstration run for the studied system with an amorphous particle at a temperature of 923 K showed that all UN fragments quickly lose nit-

rogen, which in its free form goes into a gas mixture containing argon and the remaining oxygen not attached to uranium. Such a process can actually take place due to the intense release of energy in the resulting exothermic reaction (1):

$$2UN + 2O_2 \rightarrow 2UO_2 + N_2 + \text{energy} \quad (1)$$

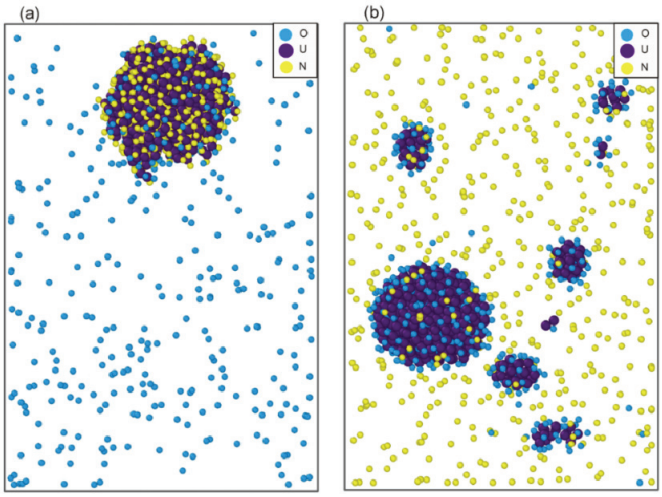


Fig. 7. *zx*-projections of the configuration of systems "amorphous fragments in a gas mixture Ar–O" at a temperature of 923 K: a) UN fragment corresponding to a time moment of 20 ps; b) $UO_x$ fragments at 685 ps.

Changing the U–N interaction to a pair interaction results in the larger UN fragment quickly breaking up into small clusters. All small clusters containing 1–3 U atoms, within a few picoseconds after changing the U–N interaction, quickly lose N atoms and acquire a small number of O atoms. Then these clusters spontaneously begin to assemble into larger $(UO_x)_n$ clusters that acquire a convex, close to spherical shape. Such clusters of different sizes are surrounded by Ar and N atoms. A small number of O atoms also remain in the gas mixture. As it can be seen from the figure, the initial UN particle is finally transformed into $(UO_x)_n$ fragments that are the final product of the model oxidation process.

The present calculations were performed with an initial oxygen content of 22.5 mol. % in the oxygen–argon mixture. The studies performed show that the completeness of the conversion of UN into uranium oxides depends on several interrelated factors. Firstly, for the progression of oxidation, the state of the particles that are exposed to oxygen is important. In particular, the structure of the particles and the state of their surface are important. It has been shown that intense oxidation of amorphous particles occurs at a lower temperature than for crystalline particles of the same size. This is facilitated by the easier fragmentation of amorphous particles compared to crystalline particles in a gaseous Ar–O

medium. The fragmentation facilitates the access of oxygen to the oxidized material. This is the rate of fragmentation of particles into smaller fragments that is mainly the limiting factor in the oxidation of UN powder.

However, the completeness of oxidation is determined not only by the increase in surface area when the integrity of the UN particle is damaged, but also by the possibility of access of oxygen atoms inside it. This possibility opens up when the U–N bonds turn out to be weaker than the U–O bonds, and the N atoms leave their positions, allowing the O atoms to form bonds with uranium. Since the rate of crushing of powder particles acts as a limiting factor for its oxidation, the completeness of this process directly depends on the size of the powder particles, as observed in the experiment.[24]

To investigate how the oxygen concentration in the Ar–O gas mixture affects the oxidation process of UN particles, similar calculations were performed in the temperature range of 923–1300 K with an oxygen concentration of 8.6 mol. % and the same amount of Ar, U and N atoms. At this lower oxygen concentration in the system, only slight fragmentation of the amorphous particle was observed, while the UN crystal retained its integrity throughout the entire calculation.

During the first 100 ps, when the effect of fragmentation of the UN particle on its oxidation is not so significant, the fraction of O atoms associated with the U atoms of the amorphous particle was ~6 % greater than for the crystalline particle. During this period, at an initial molar oxygen concentration of 22.5 mol. %, the number of formed U–O bonds for crystalline and amorphous particles exceeded these characteristics at an initial oxygen concentration of 8.6 mol. % by 2.7 and 2.9 times, respectively. It is evident that an increase in the oxygen concentration in the system significantly accelerates the process of initial oxidation.

Thus, for oxidation to occur more efficiently, it is necessary that the oxygen concentration in the gaseous mixture be as high as allowed by the design features of the experimental setup, and that the UN powder be fine and amorphous. In this case, care should be taken to ensure that the coagulation of the fine particles is inhibited. According to the results of the present work, it is advisable to execute the oxidation of UN powder at temperatures of 923–973 K, when the amorphous fraction dominates in the composition of the powder. To prevent the powder from being carried out of the chamber in which it is blown with an Ar–O gas mixture, a fine-mesh steel mesh can be used.

## CONCLUSION

This work shows that the high-temperature processing operation (in the Ar–O atmosphere) should be a single-stage process. It involves the oxidation of nitride powder from spent nuclear fuel in an atmosphere of dry oxygen and argon, converting the nitrides of fissile materials and fission products into oxides.

The process of transforming nitrides into oxides in a Ar–O gaseous mixture is largely determined by the structure of the initial nitride material. Thus, at pressures that do not lead to structural phase transitions in the UN phase (not much different from atmospheric pressure), the amorphous powder is actively oxidized at lower temperatures than the crystalline fine fraction. In order to significantly activate the oxidation of the crystalline fraction, it is necessary to increase the temperature of the system.

The fragmentation of the amorphous UN particle that occurs at lower temperatures leads to an increase in its surface area, which contributes to an increase in the intensity of oxidation. Thus, it is possible to lower the temperature at which the oxidation procedure is performed by preliminary conversion of crystalline UN particles into an amorphous state.

Realistic systems exchange mass, momentum, and/or energy with the environment, *i.e.*, they have open boundaries. The limited size of MD models, even with the use of periodic boundary conditions that expand the system, makes the comparisons with experimental results difficult. Solving this problem is the main task of MD modelling in the future.

## SUPPLEMENTARY MATERIAL

Additional data and information are available electronically at the pages of journal website: https://www.shd-pub.org.rs/index.php/JSCS/article/view/13065, or from the corresponding author on request.

*Acknowledgements*. The work is executed based on an agreement from 06.06.2023 No. 740/1199-D with JSC “Proryv”.

## ИЗВОД

## МОЛЕКУЛСКО ДИНАМИЧКА СИМУЛАЦИЈА ОКСИДАЦИЈЕ УРАНИЈУМ-НИТРИДА

ALEXANDER Y. GALASHEV[1,2], YURII P. ZAIKOV[1,2], KSENIYA A. ABRAMOVA[1,2], OKSANA R. RAKHMANOVA[1,2] и YURII S. MOCHALOV[3]

*[1]Institute of High-Temperature Electrochemistry, Ural Branch of the Russian Academy of Sciences, Yekaterinburg, Russia, [2]Ural Federal University named after the first president of Russia B.N. Yeltsin, Yekaterinburg, Russia и [3]Joint-Stock Company «Proryv», Moscow, Russia*

Извршена је молекулско динамичка симулација оксидације уранијум-мононитрида (UN) у Ar–O средини у температурском опсегу од 373–2073 K. Истраживање је урађено за UN честице кристалне и аморфне структуре при концентрацији кисеоника од 22,5 mol. % у гасној смеши. Најефикаснија оксидација аморфних честица се дешава на нижим температурама него за кристалне честице. За разлику од кристалних фрагмената, аморфне честице подлежу значајнијој фрагментицаји када се везују за кисеоник. Фрагментација UN честица је један од главних фактора који доводе до њихове оксидације. Оксидација UN честице почиње од њене површине и у случају аморфних честица дешава се брже него када су честице кристалне. Процес фрагментације честице је олакшан продирањем атома кисеоника унутар честице. Пораст концентрације кисеоника у гасној смеши подстиче процес окдиације. Структурне промене у систему су испи-

тиване помоћу парцијалне радијалне функције расподеле. Вишечестичне U–N интеракције спречавају да азот пређе у гасовито стање.

(Примљено 26. септембра, ревидирано 5. октобра, прихваћено 24. новембра 2024)

REFERENCES


1. O. A. Grigorovich, S. V. Abramov, V.I . Voronin, A. M. Potapov, M. V. Mazannikov, P. N. Mushnikov, V. Y. Shishkin, Y. P. Zajkov, A. B. Salyulev, K. R. Karimov, A. E. Dedyukhin, A. S. Kholkina, A. V. Suzdaltsev, Ru 2 732 721 C1, 22.09.2020 Bull. № 27
2. A. Sajdova, *Thesis for the degree of licentiate of engineering*, Gothenburg, 2017 (ISSN: 1652-943X)
3. C. O. T. Galvin, N. Kuganathan, N. J. Barron, R. W. Grimes, *J. Appl. Phys*. **135** (2024) 165101 (https://doi.org/10.1063/5.0177315)
4. L. Yang, N. Kaltsoyannis, *J. Nucl. Mater*. **577** (2023) 154330 (https://doi.org/10.1016/j.jnucmat.2023.154330)
5. R. Dell, V. Wheeler, E. J. Mclver, *Trans. Faraday Soc.* **62** (1966) 3591 (https://doi.org/10.1039/TF9666203591)
6. E.-Y. Choi, C. Y. Won, J.-S. Cha, W. Park, H. S. Im, S.-S. Hong, J.-M. Hur, *J. Nucl. Mater.* **444** (2014) 261 (https://doi.org/10.1016/j.jnucmat.2013.09.061)
7. Z. Da-Wei, J. H. Yu, P. Chunying, Y. Song. arXiv:1804.00095 [physics.comp-ph] (https://doi.org/10.48550/arXiv.1804.00095)
8. P. Tecmer, A. S. P. Gomes, S. Knecht, L. Visscher, *J. Chem. Phys*. **141** (2014) 041107 (https://doi.org/10.1063/1.4891801)
9. S. Zhang, F. Wang, *J. Phys. Chem., A* **121** (2017) 3966 (https://dx.doi.org/10.1021/acs.jpca.7b02985)
10. G. Liu, C. Zhang, S. M. Ciborowski, A. Asthana, L. Cheng, K. H. Bowen, *J. Phys. Chem., A* **124** (2020) 6486 (https://dx.doi.org/10.1021/acs.jpca.0c03735)
11. J. Zhao, C.-X. Chi, L.-Y. Meng, X.-L. Jiang, J. Grunenberg, H.-S. Hu, M.-F. Zhou, J. Li, W. H. Eugen Schwarz, *J. Chem. Phys.* **157** (2022) 054301 (https://doi.org/10.1063/5.0098068)
12. A. Sunaga, C. Tabata, T. Yamamura, *J. Phys. Chem., A* **126** (2022) 8606 (https://doi.org/10.1021/acs.jpca.2c05216)
13. F. Wei, G. Wu, W. H. Eugen Schwarz, J. Li, *Theor. Chem. Acc.* **129** (2011) 467 (https://doi.org/110.1007/s00214-010-0885-5)
14. L. Verlet, *Phys. Rev*. **159** (1967) 98 (https://doi.org/10.1103/PhysRev.15998)
15. V. I. Tseplyaev, S. V. Starikov, *J. Nucl. Mater*. **480** (2016) 7 (https://doi.org/10.1016/j.jnucmat.2016.07.048)
16. M. W. Cooper, N. Kuganathan, P. A. Burr, M. J.-D. Rusthon, R. W. Grimes, C. R. Stanek, D. A. Andersson, *J. Phys.* **28** (2016) 405401 (https://doi.org/10.1088/0953-8984/28/40/405401)
17. M. Krishnamurth, S. Murad, J. D. Olson, *Mol. Sim.* **32** (2006) 11 (https://doi.org/10.1080/08927020500474318)
18. K. Kurosaki, K. Yano, K. Yamada, M. Uno, S. Yamanaka, *J. Alloys Comp.* **311** (2000) 305 (https://doi.org/10.1016/S0925-8388(00)01127-0)
19. A. Y. Galashev, K. Abramova, A. Vorob'ev, O. Rakhmanova, Yu. Zaikov, *Electrochem. Mater. Technol.* **2** (2023) 20232017 (https://doi.org/10.15826/elmattech.2023.2.017)
20. A. Y. Galashev, K. A. Ivanichkina, Yu. P. Zaikov, *J. Solid State Chem*. **286** (2020) 121278 (https://doi.org/10.1016/j.jssc.2020.121278)
21. S. Plimpton, *J. Comp. Physics* **117** (1995) 1. (https://doi.org/10.1006/jcph.1995.1039)

22. V. G. Baranov, A. V. Tenishev, R. S. Kuzmin, S. A. Pokrovskiy, V. V. Mikhalchik, V. A. Astafyev, M. L. Taubin, E. S. Solntseva, *Ann. Nucl. Energy* **87** (2016) 784 (https://doi.org/10.1016/j.anucene.2014.09.023)
23. S. Zhan, J. Bao, S. Ning, M. Zhang, J.Wu, X. Wang, Y. Li, *Chem. Eng. J.* **498** (2024) 155322 (https://doi.org/10.1016/j.cej.2024.155322)
24. R. M. Dell, Y. J. Wheeler, N. J. Bridger, *Trans. Faraday Soc*. **63** (1967) 1286 (https://doi.org/10.1039/tf9676301286).